Constrained Cooperative Control for High-Order Fully Actuated Multiagent Systems With Application to Air-Bearing Spacecraft Simulators

Da-Wei Zhang, *Student Member, IEEE*, Guo-Ping Liu, *Fellow, IEEE*, and Lei Cao

***Abstract*—This article is concerned with the constrained cooperative control for high-order fully actuated multiagent systems (HOFAMASs) subject to input saturation and prescribed performance. A predictive control scheme is given to achieve constrained cooperation among HOFAMASs. In this scheme, an incremental HOFA (IHOFA) prediction model is constructed by using a Diophantine equation to replace a reduced-order one. A cost function, investigating the cooperative performance and the constraints on input saturation and prescribed performance, is optimized by multistep output predictions so that the optimal constrained cooperative controllers are developed to satisfy the consensus requirement and given constraints. The further discussion gives a condition of stability and consensus, which is convenient to check and extend in practice. Simulated and experimental results of formation control for air-bearing spacecraft simulators are shown to illustrate the effectiveness of the provided scheme.**

***Index Terms*—Constrained control, cooperative control, formation control of air-bearing spacecraft (ABS) simulators, high-order fully actuated multiagent systems (HOFAMASs), predictive control, stability and consensus.**

I. Introduction

With the worldwide acceptance of Internet of Things, multiagent systems (MASs) have become one of the most popular research works and have obtained numerous achievements in various fields, containing photovoltaic systems [1], cruise of high-speed trains [2], spacecraft flying-around [3], robotic systems [4], and other applications [5], [6], [7], [8]. Among them, cooperative control is a longstanding concern to achieve the global and individual objectives by applying a consensus control protocol, which has attracted great interests of scholars. In this topic, there are many hardware and software constraints to be considered due to the varied and complicated working conditions in practice, where unsatisfactory dynamical performances and input saturation are important factors, which seriously affect the cooperative performance, such that many teams are devoting to the solution and have obtained some previous stages (see [9], [10], [11], and other related studies).

To overcome the influences of input saturation on cooperative performance, a lot of scholars have obtained many useful results. For example, Qi et al. [12] use both eigenvalues of the Laplace matrix of the communication network and sampling period to give a necessary and sufficient condition of consensus under input saturation. Wang et al. [13] propose a multiple saturation framework based on a switched parametric Lyapunov function and a three-layer nodes model to realize the semiglobal tracking cooperative control. In [14], an event-triggering control combined with an adaptive neural network is provided to cope with the input saturation and other constraints so that the input saturation can be overcome by Nussbaum-type function and mean-value theorems. In [15], a gain scheduled method is given to implement the leader–follower consensus subject to input saturation; this method constructs a time-variant gain state feedback and a parametric scheduler to achieve and accelerate the consensus tracking. Lv et al. [16] present two distributed adaptive antisaturation protocols based on edge and node, the proposed protocols depend on an integrated antisaturation observer such that the consensus is guaranteed. Additionally, [17], [18], and[19] and other related results also provide some feasible approaches to deal with input constraints, which can be extended to the cooperative control of MASs under input saturation.

To improve the dynamical performances in the cooperative control (mainly containing overshoot and convergence rate), prescribed performance control, first proposed in [20], can make the tracking error converge to a preset allowable range and guarantee that the overshoot and convergence rate satisfy a prescribed condition. Different from the work in [21] and [22], prescribed performance control relaxes the requirements of steady tracking errors and pays more attention to the improvement of dynamical performances. In the cooperative control

Manuscript received 19 July 2022; revised 5 October 2022; accepted 17 November 2022. Date of publication 30 November 2022; date of current version 16 June 2023. Recommended by Technical Editor A. Alanis and Senior Editor M. Basin. This work was supported by the National Natural Science Foundation of China under Grant 62173255 and Grant 62188101. *(Corresponding author: Guo-Ping Liu.)*

Da-Wei Zhang and Lei Cao are with the Center for Control Theory and Guidance Technology, Harbin Institute of Technology, Harbin 150001, China (e-mail: zhangdawei@stu.hit.edu.cn; 18b904027@stu.hit.edu.cn).

Guo-Ping Liu is with the Center for Control Theory and Guidance Technology, Harbin Institute of Technology, Harbin 150001, China, and also with the Center for Control Science and Technology, Southern University of Science and Technology, Shenzhen 518055, China (e-mail: liugp@sustech.edu.cn).

Color versions of one or more figures in this article are available at https://doi.org/10.1109/TMECH.2022.3223927.

Digital Object Identifier 10.1109/TMECH.2022.3223927

of MASs, Yang et al. [23] apply an active disturbance rejection control approach to implement the time-variant formation with prescribed performance. Chen and Dimarogonas [24] use prescribed performance guarantees to consider a leader–follower formation control aiming at first-order and second-order cases and it proposes a backstepping approach to realize the target formation within the prescribed performance bounds. Ren et al. [25] propose a speed function to ensure the prescribed tracking performance so that the bipartite consensus can be realized by an adaptive event-triggering algorithm. Liang et al. [26] also design a speed function that makes the tracking errors converge to a preset compact set; then, the cooperative controller is solved by backstepping method and Lyapunov theories. Liu and Yang [27] present an adaptive observer to decouple the controllers by using Nussbaum functions, such that the consensus errors converge to the prescribed performance interval. In addition, there are also other research works for this issue (see [28], [29], [30], and relative studies).

A limitation of the above is that they almost always utilize the traditional first-order state-space model to describe the dynamical behaviors of MASs, which causes the loss of practical meanings of physical systems and increases the design difficulties. Following the idea in [31], the HOFA system, a new system representation for control design, is used to be a common model for most physical systems. Different from the traditional model, the HOFA system has a clear physical background and guarantees the full actuation characteristic of practical systems, it also effectively simplifies the control design and avoids some shortcomings in model reduction, such as ill-conditioned matrices and unstable numerical solutions. Predictably, the HOFA model for MASs will open up an interesting and new research field about the synthesis of MASs and other relative research works; however, it is still a gap at present. Cooperative control for MASs with cyberattacks, game theories, communication constraints, and their associated problems will be re-established and resolved. Our team has obtained some preliminary results on the cooperative control for HOFAMASs (see [32], [33], and [34]). Compared to that in [32], this study achieves cooperation via the optimization of a cost function considering cooperative performance rather than a nonoptimized feedback control. Different from the work in [33], this study considers a cooperative control of HOFAMASs subject to input saturation and prescribed performance instead of a constraint-free one. Based on the realization of cooperation, this study pays more attention to the avoidance of input saturation and the improvement of dynamical performances while Zhang et al. [34] focus on the active compensation of communication delays. In this study, a key problem is to propose an HOFA control to handle the input saturation and prescribed performance during the cooperation and another is to ensure stability and consensus.

Of various approaches, predictive control can not only realize the cooperative control but also deal with many hardware and software constraints during the cooperation, which has obtained a string of results (see [35], [36], and [37]). For HOFAMASs with input saturation and prescribed performance, this research gives a predictive control scheme to achieve the constrained cooperative control among HOFAMASs. The major contributions are drawn as follows. First, a predictive control scheme is considered to achieve the constrained cooperative control of HOFAMASs. Concretely, an IHOFA prediction model is constructed via a Diophantine equation to construct the multistep output predictions. Furthermore, the given constraints on input saturation and prescribed performance are transformed into two inequality constraints in an optimization problem so that the constrained cooperative control problem can be converted into a constrained optimization one. By applying a constrained optimization algorithm, a feasible solution is solved to realize the constrained cooperative control and satisfy the given constraints. Then, a criterion of stability and consensus is derived, which is simple to check and extend in practice. Moreover, a formation control experiment of three air-bearing spacecraft (ABS) simulators is taken to prove the effectiveness of the theoretical result. The highlights of this research are concluded as follows:

1) An HOFA model is applied to describe the dynamical behaviors of MASs, which considers the multidimension vector and high-order difference equation of state variables.
2) An IHOFA prediction model is constructed via a Diophantine equation instead of a reduced-order one so that the design of predictive control is decided and expressed in HOFA form.
3) The prescribed performance condition can be converted into an inequality constraint such that the multiple derivative computations of error in [20] can be avoided, which reduces the computational complexity in the process of error transformation.

Throughout this article, $\|\cdot\|$ is the Euclidean norm, and $\hat{s}(k+i|k)$ denotes the ith ahead prediction of $s(k)$ based on k time. $N_y \geq N_u$ indicates the output and control prediction horizons. $\Delta = 1 - q^{-1}$ represents the difference operator where q is a time operator satisfied $s(k+i) = q^i s(k)$, $i \in \mathbb{Z}$ (see [38]).

II. Problem Statement

The constrained cooperative control of HOFAMASs subject to input saturation and prescribed performance is shown in Fig. 1, its topology is described as a digraph $\mathcal{G} = \{\mathcal{N}, \mathcal{E}, \mathcal{W}\}$, given in Definition 1.

Definition 1: In the graph $\mathcal{G}$, $\mathcal{N} = \{1, 2, \ldots, N\}$ is the set of all HOFAMASs, $\mathcal{E} \subset \mathcal{N} \times \mathcal{N}$ indicates the set of edges, $\mathcal{W} = \{w_{ij}\}$ represents an adjacency matrix with $w_{ij} \geqq 0$ and $w_{ii} = 0$. The $(i, j) \in \mathcal{E}$ implies the ith HOFAMAS receives the data from the jth one via the network by means of w_{ij}. $\mathcal{N}_i = \{j | j \in \mathcal{N}, j \neq i\}$.

From [33], the ith HOFAMAS is proposed as

$$\begin{aligned} x_i(k+n) &= -\sum_{l=0}^{n-1} A_{il} x_i(k+l) + B_i u_i(k) \\ y_i(k) &= C_i x_i(k) \end{aligned} \tag{1}$$

where $i \in \mathcal{N}$, x_i, $u_i \in \mathbb{R}^{n_i}$, $y_i \in \mathbb{R}^m$ denote the state, input, and output vectors of the ith HOFAMAS, $A_{il} \in \mathbb{R}^{n_i \times n_i}$, $B_i \in \mathbb{R}^{n_i \times n_i}$, $C_i \in \mathbb{R}^{m \times n_i}$ are known coefficient matrices, and

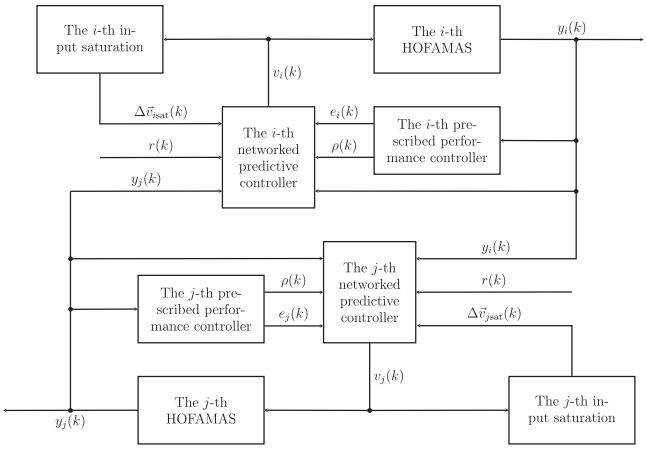

Fig. 1. Constrained cooperative control of HOFAMASs subject to input saturation and prescribed performance.

$\det(B_i) \neq 0$. For HOFAMAS (1), some assumptions are presented as follows.

Assumption 1:

A1: State vector of HOFAMAS (1) is available.

A2: $\mathcal{G}$ is a fixed communication topology and $\mathcal{W}$ is a constant adjacency matrix.

A3: The clock is synchronized and there exists a timestamp when transmitting data.

Considering the practice on site, a saturation constraint on control input is considered as

$$u_{\min} \leq u_i(k) \leq u_{\max} \tag{2}$$

where $u_{\min}$ and $u_{\max}$ are the minimum and maximum of control input, respectively. Let the tracking error $e_i(k)$ be $e_i(k) = y_i(k) - r(k)$, where $r(k)$ is a given reference for HOFAMASs. Combining with the prescribed performance control approach, a constraint on dynamical performance is given as

$$-\rho(k) \leq e_i(k) \leq \rho(k) \tag{3}$$

where $\rho(k)$ is a performance boundary function. Then, a fully actuated control for HOFAMAS (1) is designed as

$$u_i(k) = B_i^{-1} v_i(k)$$

where $v_i(k)$ is the actual control input designed by predictive control and B_i^{-1} is a given feedback coefficient; then, system (1) is transformed into

$$x_i(k+n) = -\sum_{l=0}^{n-1} A_{il} x_i(k+l) + v_i(k). \tag{4}$$

For cooperation, a cost function is given as

$$J(k) = \sum_{i \in \mathcal{N}} J_i(k) \tag{5}$$

where $J_i(k)$ indicates a subobjective associated with the cooperative performance of the ith HOFAMAS.

Problem 1: Given HOFAMAS (1) satisfying Assumption 1, this research is to develop a predictive control $v_i(k)$ satisfied constraints (2) and (3) by optimizing (5) to realize the stability and consensus of system (4), such that the following statements hold.

C1: For a given reference $r(k)$, if $\|r(k)\| < \infty$, $\|y_i(k)\| < \infty \quad \forall k \geq 0$.

C2: $\lim_{k\to\infty} \|y_i(k) - y_j(k)\| = 0$, $i \in \mathcal{N}$, $j \in \mathcal{N}_i$.

III. Predictive Control Scheme for Constrained Cooperative Control

A. Multistep Output Prediction

By using the q operator, system (4) can be represented by

$$A_i(q^{-1}) x_i(k) = B_i(q^{-1}) v_i(k-1) \tag{6}$$

where $A_i(q^{-1}) = \sum_{l=0}^{n-1} A_{il} q^{l-n} + I$, $B_i(q^{-1}) = q^{1-n}$. Meanwhile, a Diophantine equation is presented as follows:

$$E_{i,l}(q^{-1}) A_i \Delta + q^{-j} F_{i,l}(q^{-1}) = I \tag{7}$$

where $E_{i,l}$ and $F_{i,l}$ are polynomial matrices depended on both prediction horizon l and system coefficient $A_i(q^{-1})$, given as

$$E_{i,l}\left(q^{-1}\right) = e_{i,l,0} + e_{i,l,1} q^{-1} + \cdots + e_{i,l,l-1} q^{-(l-1)}$$
$$F_{i,l}\left(q^{-1}\right) = f_{i,l,0} + f_{i,l,1} q^{-1} + \cdots + f_{i,l,n} q^{-n}.$$

Multiplying $E_{i,l}\Delta q^l$ at (6) has

$$E_{i,l} A_i \Delta x_i(k+l) = E_{i,l} B_i \Delta v_i(k+l-1)$$

combining with (7) constructs an IHOFA prediction model as

$$x_i(k+l) = F_{i,l} x(k) + G_{i,l} \Delta v_i(k+l-1) \tag{8}$$

with $G_{i,l} = E_{i,l} B_i = g_{i,l,0} + g_{i,l,1} q^{-1} + \cdots + g_{i,l,n+l-2} q^{2-n-l}$.

Based on (8), the ahead prediction of $x_i(k)$ is derive as

$$\hat{x}_i(k+1|k) = F_{i,1} x_i(k) + G_{i,1} \Delta \hat{v}_i(k|k)$$
$$\vdots$$
$$\hat{x}_i(k+N_y|k) = F_{i,N_y} x_i(k) + G_{i,N_y} \Delta \hat{v}_i(k+N_y-1|k)$$

then output prediction is obtained as

$$\hat{y}_i(k+l|k) = C_i \hat{x}_i(k+l|k),\ l = 1, 2, \ldots, N_y \tag{9}$$

when $l = N_u + 1, N_u + 2, \ldots, N_y$, $\hat{v}_i(k+l|k) = \hat{v}_i(k+N_u|k)$ so that $\Delta\hat{v}_i(k+l|k) = 0$, thus (9) can be compactly transformed into

$$\hat{Y}_i(k+N_y|k) = P_{i1} x_i(k) + P_{i2} \Delta \hat{V}_i(k+N_u|k) \tag{10}$$

where

$$\hat{Y}_i(k+N_y|k) = \left[\hat{y}_i^{\mathrm{T}}(k+N_y|k) \quad \cdots \quad \hat{y}_i^{\mathrm{T}}(k+1|k)\right]^{\mathrm{T}}$$
$$\Delta\hat{V}_i(k+N_u|k) = \left[\Delta\hat{v}_i^{\mathrm{T}}(k+N_u|k) \quad \cdots \quad \Delta\hat{v}_i^{\mathrm{T}}(k|k)\right]^{\mathrm{T}}$$

and

$$P_{i1}=C_i\begin{bmatrix}F_{i,N_y}\\ \vdots\\ F_{i,N_u+1}\\ F_{i,N_u}\\ \vdots\\ F_{i,1}\end{bmatrix},P_{i2}=C_i\begin{bmatrix}G_{i,N_y} & 0 & \cdots & 0\\ \vdots & \vdots & \cdots & \vdots\\ G_{i,N_u+1} & 0 & \cdots & 0\\ 0 & G_{i,N_u} & \ddots & \vdots\\ \vdots & \ddots & \ddots & 0\\ 0 & \cdots & 0 & G_{i,1}\end{bmatrix}.$$

In addition, an incremental constraint is defined by

$$\Delta\hat{v}_i(k+l|k)=\gamma_{il}\Delta\hat{v}_i(k|k) \tag{11}$$

where $\gamma_{il}>0$, $l=1,2,\ldots,N_u$, is the weighted coefficient; hence, P_{i2} can be degenerated by

$$P_{i3}=P_{i2}\Gamma_i,\ \Gamma_i=\text{Blockdiag}\{\gamma_{N_u}I,\ldots,\gamma_1 I,I\}.$$

B. Constraints Transformation

Following our previous result in [39], constraint (2) yields

$$\begin{aligned}&B_iu_{\min}\le v_i(k)\le B_iu_{\max}\\ &B_iu_{\min}\le\hat{v}_i(k+1|k)\le B_iu_{\max}\\ &\qquad\vdots\\ &B_iu_{\min}\le\hat{v}_i(k+N_u|k)\le B_iu_{\max}.\end{aligned}$$

Let $v_{i\min}=B_iu_{\min}$ and $v_{i\max}=B_iu_{\max}$, further

$$\begin{aligned}&v_{i\min}-v_i(k-1)\le\Delta\hat{v}_i(k|k)\le v_{i\max}-v_i(k-1)\\ &v_{i\min}-v_i(k-1)\le\sum_{l=0}^{1}\Delta\hat{v}_i(k+l|k)\le v_{i\max}-v_i(k-1)\\ &\qquad\vdots\\ &v_{i\min}-v_i(k-1)\le\sum_{l=0}^{N_u}\Delta\hat{v}_i(k+l|k)\le v_{i\max}-v_i(k-1)\end{aligned}$$

denote $\Delta v_{i\min}(k)=v_{i\min}-v_i(k-1)$, $\Delta v_{i\max}(k)=v_{i\max}-v_i(k-1)$ and

$$\Delta\vec{v}_{i\min}(k)=\begin{bmatrix}\Delta v_{i\min}(k)\\ \vdots\\ \Delta v_{i\min}(k)\end{bmatrix},\Delta\vec{v}_{i\max}(k)=\begin{bmatrix}\Delta v_{i\max}(k)\\ \vdots\\ \Delta v_{i\max}(k)\end{bmatrix}$$

then the above is derived that

$$\Delta\vec{v}_{i\min}(k)\le B_{v0}\Delta\hat{V}_i(k+N_u|k)\le\Delta\vec{v}_{i\max}(k)$$

with $B_{v0}=\begin{bmatrix}I & \cdots & I\\ & \ddots & \vdots\\ & & I\end{bmatrix}$, such that

$$B_{s0}\Delta\hat{V}_i(k+N_u|k)\le\Delta\vec{v}_{i\text{sat}}(k) \tag{12}$$

where $B_{s0}=\begin{bmatrix}-B_{v0}\\ B_{v0}\end{bmatrix}$ and $\Delta\vec{v}_{i\text{sat}}(k)=\begin{bmatrix}-\Delta\vec{v}_{i\min}(k)\\ \Delta\vec{v}_{i\max}(k)\end{bmatrix}$. Considering (11), B_{v0} is degenerated as $B_{v1}=B_{v0}\Gamma_i$ and $B_{s1}=\begin{bmatrix}-B_{v1}\\ B_{v1}\end{bmatrix}$.

Similarly, constraint (3) also obtains

$$\begin{aligned}&-\rho(k+1)\le\hat{e}_i(k+1|k)\le\rho(k+1)\\ &\qquad\vdots\\ &-\rho(k+N_y)\le\hat{e}_i(k+N_y|k)\le\rho(k+N_y)\end{aligned}$$

where $\hat{e}_i(k+l|k)=\hat{y}_i(k+l|k)-r(k+l)$, $l=1,2,\ldots,N_y$, such that

$$B_{e1}\hat{E}_i(k+N_y|k)\le B_{e2}\varrho(k+N_y) \tag{13}$$

with $B_{e1}=[-I\quad I]^{\mathrm{T}}$, $B_{e2}=[I\quad I]^{\mathrm{T}}$, $\hat{E}_i(k+N_y|k)=\hat{Y}_i(k+N_y|k)-R(k+N_y)$ and

$$\begin{aligned}R(k+N_y)&=\begin{bmatrix}r^{\mathrm{T}}(k+N_y) & \cdots & r^{\mathrm{T}}(k+1)\end{bmatrix}^{\mathrm{T}}\\ \varrho(k+N_y)&=\begin{bmatrix}\rho^{\mathrm{T}}(k+N_y) & \cdots & \rho^{\mathrm{T}}(k+1)\end{bmatrix}^{\mathrm{T}}.\end{aligned}$$

C. Solve the Optimal Predictive Control Increment

For the cooperative performance for the ith HOFAMAS, a subobjective $J_i(k)$ in (5) is defined as

$$\begin{aligned}J_i(k)=&\sum_{j\in\mathcal{N}_i}w_{ij}\|\hat{Y}_i(k+N_y|k)-\hat{Y}_j(k+N_y|k)\|^2\\ &+b_i\|\hat{E}_i(k+N_y|k)\|^2+c_i\|\Delta\hat{V}_i(k+N_u|k)\|^2\end{aligned} \tag{14}$$

where w_{ij} is the (i,j)th element of the adjacency matrix $\mathcal{W}$, and b_i, c_i are positive numbers and weighted coefficients, respectively. In (14), the first item pays attention to the cooperative performance of HOFAMASs, the second item focuses on the difference between given reference and output prediction, and the third one gives a limitation about predictive control increment, which is realistic in practical applications.

To solve the constrained cooperative control for Problem 1, an optimized problem is proposed as follows:

$$\begin{aligned}&\min J_i(k)\\ &\text{s.t. (12), (13).}\end{aligned}$$

By using a constrained optimized algorithm based on matrix inverse decomposition in [40], $J_i(k)$ should first be replaced by $J_i'(k)$, established as

$$\begin{aligned}J_i'(k)=&J_i(k)+\alpha_i\|B_{e1}\hat{E}_i(k+N_y|k)-B_{e2}\varrho(k+N_y)\|^2\\ &+\beta_i\|B_{s0}\Delta\hat{V}_i(k+N_u|k)-\Delta\vec{v}_{i\text{sat}}(k)\|^2\end{aligned} \tag{15}$$

where α_i, β_i are positive numbers and weighted coefficients, respectively; then, the above constrained optimized problem can be converted into a constraint-free one, that is, $\min J_i'(k)$. Then, for the optimal predictive control increment $\Delta v_i(k)$, let

$$\frac{\partial}{\partial\Delta\hat{V}_i(k+N_u|k)}J(k)=0\quad\forall i\in\mathcal{N}$$

combining (10) with (15) has

$$\sum_{j\in\mathcal{N}_i} w_{ij}P_{i3}^{\mathrm{T}}\Big(P_{i1}x_i(k)+P_{i3}\Delta\hat{V}_i(k+N_u|k)-P_{j1}x_j(k)$$
$$-P_{j3}\Delta\hat{V}_j(k+N_u|k)\Big)+b_iP_{i3}^{\mathrm{T}}\Big(P_{i1}x_i(k)+P_{i3}\Delta\hat{V}_i(k+N_u|k)$$
$$-R(k+N_y))+c_i\Delta\hat{V}_i(k+N_u|k)+\alpha_iP_{i3}^{\mathrm{T}}B_{e1}^{\mathrm{T}}\left(B_{e1}P_{i1}x_i(k)\right.$$
$$\left.+B_{e1}P_{i3}\Delta\hat{V}_i(k+N_u|k)-B_{e1}R(k+N_y)-B_{e2}\varrho(k+N_y)\right)$$
$$+\beta_iB_{s1}^{\mathrm{T}}\Big(B_{s1}\Delta\hat{V}_i(k+N_u|k)-\Delta\vec{v}_{i\mathrm{sat}}(k)\Big)=0$$

such that

$$\Delta\hat{V}(k+N_u|k)=F^{-1}Gx(k)+F^{-1}SR(k+N_y)$$
$$+F^{-1}M\varrho(k+N_y)+F^{-1}Q\Delta\vec{v}_{\mathrm{sat}}(k) \quad (16)$$

where

$$\Delta\hat{V}(k+N_u|k)=\left[\Delta\hat{V}_1^{\mathrm{T}}(k+N_u|k)\ \cdots\ \Delta\hat{V}_N^{\mathrm{T}}(k+N_u|k)\right]^{\mathrm{T}}$$
$$x(t)=\left[x_1^{\mathrm{T}}(k)\ \cdots\ x_N^{\mathrm{T}}(k)\right]^{\mathrm{T}}$$
$$\Delta\vec{v}_{\mathrm{sat}}(k)=\left[\Delta\vec{v}_{1\mathrm{sat}}^{\mathrm{T}}(k)\ \cdots\ \Delta\vec{v}_{N\mathrm{sat}}^{\mathrm{T}}(k)\right]^{\mathrm{T}}$$

and

$$F=\{f_{ij}\},\ f_{ij}=-w_{ij}P_{i3}^{\mathrm{T}}P_{j3}$$
$$f_{ii}=(w_i+b_i)P_{i3}^{\mathrm{T}}P_{i3}+\alpha_iP_{i3}^{\mathrm{T}}B_{e1}^{\mathrm{T}}B_{e1}P_{i3}+\beta_iB_{s1}^{\mathrm{T}}B_{s1}+c_iI$$
$$G=\{g_{ij}\},\ g_{ij}=w_{ij}P_{i3}^{\mathrm{T}}P_{j1}$$
$$g_{ii}=-(w_i+b_i)P_{i3}^{\mathrm{T}}P_{i1}-\alpha_iP_{i3}^{\mathrm{T}}B_{e1}^{\mathrm{T}}B_{e1}P_{i1}$$
$$S=\begin{bmatrix}b_1P_{13}^{\mathrm{T}}+\alpha_1P_{13}^{\mathrm{T}}B_{e1}^{\mathrm{T}}B_{e1}\\ \vdots\\ b_NP_{N3}^{\mathrm{T}}+\alpha_NP_{N3}^{\mathrm{T}}B_{e1}^{\mathrm{T}}B_{e1}\end{bmatrix},M=\begin{bmatrix}\alpha_1P_{13}^{\mathrm{T}}B_{e1}^{\mathrm{T}}B_{e2}\\ \vdots\\ \alpha_NP_{N3}^{\mathrm{T}}B_{e1}^{\mathrm{T}}B_{e2}\end{bmatrix}$$
$$Q=\mathrm{Blockdiag}\{\beta_1B_{s1}^{\mathrm{T}},\ldots,\beta_NB_{s1}^{\mathrm{T}}\},w_i=\sum_{j\in\mathcal{N}_i}w_{ij}$$

thus, the optimal solution of predictive control increment for the ith HOFAMAS is computed by $\Delta v_i(k)=\Delta\hat{v}_i(k|k)=H_i\Delta\hat{V}(k+N_u|k)$, given as

$$\Delta v_i(k)=H_iF^{-1}Gx(k)+H_iF^{-1}SR(k+N_y)$$
$$+H_iF^{-1}M\varrho(k+N_y)+H_iF^{-1}Q\Delta\vec{v}_{\mathrm{sat}}(k) \quad (17)$$

where $H_i\in\mathbb{R}^{n_i\times(N_u+1)\tilde{n}}$, $\tilde{n}=\sum_{i=1}^{N}n_i$, denotes a coefficient matrix whose $(N_u+1)i$th column is an identity matrix and others are zeros.

Remark 1: When there are no constraints during the cooperation, predictive control increment is computed by optimizing (14), given as

$$\Delta\hat{V}_0(k+N_u|k)=F_0^{-1}G_0x(k)+F_0^{-1}S_0R(k+N_y)$$

where F_0, G_0, and S_0 are produced by setting $\alpha_i=\beta_i=0$ in F, G, and S in (16). Furthermore, it is derived that $f_{ii}=f_{0,ii}+\Xi_i^{\mathrm{T}}\Lambda_i\Xi_i$, where $\Xi_i^{\mathrm{T}}=[\ P_{i3}^{\mathrm{T}}B_{e1}^{\mathrm{T}}\quad B_{s1}^{\mathrm{T}}\ ]$ and $\Lambda_i=\mathrm{Blockdiag}\{\alpha_iI,\beta_iI\}$, such that $F=F_0+\Xi^{\mathrm{T}}\Lambda\Xi$ with $\Xi=\mathrm{Blockdiag}\{\Xi_1,\ldots,\Xi_N\}$ and $\Lambda=\mathrm{Blockdiag}\{\Lambda_1,\ldots,\Lambda_N\}$. Based on matrix inverse decomposition, it is obtained as

$$F^{-1}=F_0^{-1}-F_0^{-1}\Xi^{\mathrm{T}}\left(\Xi F_0^{-1}\Xi^{\mathrm{T}}+\Lambda^{-1}\right)^{-1}\Xi F_0^{-1}.$$

Furthermore, constraints (12) and (13) are rewritten as an unified form as

$$\Upsilon_i\geq\Xi_i\Delta\hat{V}_{0i}(k+N_u|k)$$
$$\Upsilon_i=\begin{bmatrix}B_{e2}\varrho(k+N_y)+B_{e1}R(k+N_y)-B_{e1}P_{i1}x_i(k)\\ \Delta\hat{v}_{i\mathrm{sat}}\end{bmatrix}$$

and $\Xi\Delta\hat{V}_0(k+N_u|k)\leq\Upsilon$, $\Upsilon=\mathrm{Blockdiag}\{\Upsilon_1,\ldots,\Upsilon_N\}$. In this view, (16) is also rewritten as

$$\Delta\hat{V}(k+N_u|k)$$
$$=F^{-1}\left(G_0x(k)+S_0R(k+N_y)+\Xi^{\mathrm{T}}\Lambda\Upsilon\right)$$
$$=F_0^{-1}\Big(F_0\Delta\hat{V}_0(k+N_u|k)\Big)+F_0^{-1}\Xi^{\mathrm{T}}\Lambda\Upsilon$$
$$-F_0^{-1}\Xi^{\mathrm{T}}\left(\Xi F_0^{-1}\Xi^{\mathrm{T}}+\Lambda^{-1}\right)^{-1}\Xi F_0^{-1}\Big(F_0\Delta\hat{V}_0(k+N_u|k)\Big)$$
$$-F_0^{-1}\Xi^{\mathrm{T}}\left(\Xi F_0^{-1}\Xi^{\mathrm{T}}+\Lambda^{-1}\right)^{-1}\Xi F_0^{-1}\Xi^{\mathrm{T}}\Lambda\Upsilon$$
$$=\Delta\hat{V}_0(k+N_u|k)+F_0^{-1}\Xi^{\mathrm{T}}\left(\Xi F_0^{-1}\Xi^{\mathrm{T}}+\Lambda^{-1}\right)^{-1}\Upsilon$$
$$-F_0^{-1}\Xi^{\mathrm{T}}\left(\Xi F_0^{-1}\Xi^{\mathrm{T}}+\Lambda^{-1}\right)^{-1}\Xi\Delta\hat{V}_0(k+N_u|k)$$
$$=\Delta\hat{V}_0(k+N_u|k)$$
$$-F_0^{-1}\Xi^{\mathrm{T}}\left(\Xi F_0^{-1}\Xi^{\mathrm{T}}+\Lambda^{-1}\right)^{-1}\Big(\Xi\Delta\hat{V}_0(k+N_u|k)-\Upsilon\Big)$$

which means the feasibility for the optimal solution of (15) can be guaranteed and improved by using the optimal solution of (14) to subtract an additional item when taking the critical equality constraints of (14) into (15). More details are given in [40].

IV. Stability and Consensus Analysis

The feasibility for the optimal solution of $\Delta v_i(k)$ has been illustrated in Remark 1, so stability and consensus of system (4) in this study will be discussed under the feasible solution. Let $A_{ic}=A_i^{-1}(q^{-1})B_i^{-1}(q^{-1}),r(\cdot)=r,\rho(\cdot)=\rho$. Clearly, $\Delta\vec{v}_{i\mathrm{sat}}(k)$ is also written as

$$\Delta\vec{v}_{i\mathrm{sat}}(k)=\left[-\Delta\vec{v}_{i\min}^{\mathrm{T}}(k)\quad\Delta\vec{v}_{i\max}^{\mathrm{T}}(k)\right]^{\mathrm{T}}$$
$$=\left[-\Delta v_{i\min}^{\mathrm{T}}(k)\ \cdots\ -\Delta v_{i\min}^{\mathrm{T}}(k)\right.$$
$$\left.\Delta v_{i\max}^{\mathrm{T}}(k)\ \cdots\ \Delta v_{i\max}^{\mathrm{T}}(k)\ \right]^{\mathrm{T}}$$
$$=\sigma_{i1}v_i(k-1)+\sigma_{i2}\vec{u}_{\mathrm{sat}}$$

where $\vec{u}_{\mathrm{sat}}=[u_{\min}^{\mathrm{T}}\quad u_{\max}^{\mathrm{T}}]^{\mathrm{T}}$ and

$$\sigma_{i1}=\left[I\ \cdots\ I\ -I\ \cdots\ -I\right]^{\mathrm{T}}$$
$$\sigma_{i2}=\begin{bmatrix}-B_i&\cdots&-B_i&0&\cdots&0\\ 0&\cdots&0&B_i&\cdots&B_i\end{bmatrix}^{\mathrm{T}}$$

then

$$\begin{aligned}\Delta\vec{v}_{\text{sat}}(k) &= \left[\Delta\vec{v}_{1\text{sat}}^{\mathrm{T}}(k) \quad \cdots \quad \Delta\vec{v}_{N\text{sat}}^{\mathrm{T}}(k)\right]^{\mathrm{T}} \\ &= \Sigma_1 v(k-1) + \Sigma_2 \vec{u}_{\text{sat}}\end{aligned}$$

where $v(k-1) = [\ v_1^{\mathrm{T}}(k-1) \ \cdots \ v_N^{\mathrm{T}}(k-1)\ ]^{\mathrm{T}}$, $\Sigma_1 = \text{Blockdiag}\{\sigma_{11}, \ldots, \sigma_{N1}\}$, $\Sigma_2 = [\ \sigma_{12}^{\mathrm{T}} \ \cdots \ \sigma_{N2}^{\mathrm{T}}\ ]^{\mathrm{T}}$. Thus, in (17), $\Delta v_i(k)$ is rewritten as

$$\begin{aligned}\Delta v_i(k) &= H_i F^{-1} G x(k) + H_i F^{-1} S R(k+N_y) \\ &\quad + H_i F^{-1} M \varrho(k+N_y) + H_i F^{-1} Q \Sigma_1 v(k-1) \\ &\quad + H_i F^{-1} Q \Sigma_2 \vec{u}_{\text{sat}}\end{aligned}$$

let $\Delta v(k) = [\ \Delta v_1^{\mathrm{T}}(k) \ \cdots \ \Delta v_N^{\mathrm{T}}(k)\ ]^{\mathrm{T}}$ so that

$$\begin{aligned}\Delta v(k) &= H_G x(k) + H_S R(k+N_y) + H_M \varrho(k+N_y) \\ &\quad + H_{Q1} v(k-1) + H_{Q2} \vec{u}_{\text{sat}} \\ &= H_G \Delta x(k) + (H_{Q1} + I)\Delta v(k-1) \qquad (18)\end{aligned}$$

with

$$H_G = \begin{bmatrix} H_1 F^{-1} G \\ \vdots \\ H_N F^{-1} G \end{bmatrix}, H_S = \begin{bmatrix} H_1 F^{-1} S \\ \vdots \\ H_N F^{-1} S \end{bmatrix}$$

$$H_M = \begin{bmatrix} H_1 F^{-1} M \\ \vdots \\ H_N F^{-1} M \end{bmatrix}, H_{Qi} = \begin{bmatrix} H_1 F^{-1} Q \Sigma_i \\ \vdots \\ H_N F^{-1} Q \Sigma_i \end{bmatrix},\ i = 1, 2.$$

Let $\Delta x(k) = [\ \Delta x_1^{\mathrm{T}}(k) \ \cdots \ \Delta x_N^{\mathrm{T}}(k)\ ]^{\mathrm{T}}$, combining with (18) obtains

$$\begin{aligned}\Delta x(k+1) &= A_c \Delta v(k) \\ &= A_G x(k) + A_S R(k+N_y) \\ &\quad + A_M \varrho(k+N_y) + A_{Q1} v(k-1) + A_{Q2} \vec{u}_{\text{sat}} \\ &= (A_G + I)\Delta x(k) + A_{Q1}\Delta v(k-1) \qquad (19)\end{aligned}$$

where $A_c = \text{Blockdiag}\{A_{1c}, \ldots, A_{Nc}\}$, $A_G = A_c H_G$, $A_S = A_c H_S$, $A_M = A_c H_M$, $A_{Q1} = A_c H_{Q1}$, $A_{Q2} = A_c H_{Q2}$. Denote $\xi(k) = [\ \Delta x^{\mathrm{T}}(k) \quad \Delta v^{\mathrm{T}}(k-1)\ ]^{\mathrm{T}}$, systems (18) and (19) are compactly formulated as

$$\xi(k+1) = \Phi\xi(k),\ \Phi = \begin{bmatrix} A_G + I & A_{Q1} \\ H_G & H_{Q1} + I \end{bmatrix}. \qquad (20)$$

Theorem 1: System (4) realizes the stability and consensus if and only if system (20) achieves the asymptotic stability (AS).

Proof: If system (4) realizes the stability and consensus, Conditions C1–C2 are satisfied, and hence, $\Delta x_i(k) \to 0$ as $k \to \infty$, which derives $\Delta v_i(k-1) \to 0$ as $k \to \infty$ because of (6), such that $\Delta x(t) \to 0$ and $\Delta v(k-1) \to 0$ as $k \to \infty$, and hence, system (20) achieves the AS.

If system (20) achieves the AS, $\xi(k) \to 0$ as $k \to \infty$, which means $\Delta x(k) \to 0$ and $\Delta v(k-1) \to 0$ as $k \to \infty$. $\Delta x(k) \to 0$ implies that system (4) realizes the bounded stability, thus Condition C1 is satisfied. Meanwhile, combining (10) with (11) has

$$\begin{aligned}\hat{Y}_i(k+N_y|k) &= P_{i1} x_i(k) + P_{i3}\Delta\hat{V}_i(k|k) \\ B_{s0}\Delta\hat{V}_i(k+N_u|k) &= B_{s1}\Delta\hat{V}_i(k|k)\end{aligned}$$

where $\Delta\hat{V}_i(k|k) = [\ \Delta\hat{v}_i^{\mathrm{T}}(k|k) \ \cdots \ \Delta\hat{v}_i^{\mathrm{T}}(k|k)\ ]^{\mathrm{T}}$. Because of $\Delta v(k-1) = 0, \Delta v(k) = 0$, thus $\Delta\hat{V}_i(k|k) = 0$, then $\hat{Y}_i(k+N_y|k) = P_{i1} x_i(k)$ and $\Delta\vec{v}_{i\text{sat}}(k) = B_{s1}\Delta\hat{V}_i(k|k) = 0$. Based on (17), $Gx(k) + SR(k+N_y) + M\varrho(k+N_y) = 0$, it yields

$$\begin{bmatrix} g_{11} & g_{12} & \cdots & g_{1N} \\ g_{21} & g_{22} & \cdots & g_{2N} \\ \vdots & \vdots & \ddots & \vdots \\ g_{N1} & g_{N2} & \cdots & g_{NN} \end{bmatrix} \begin{bmatrix} x_1(k) \\ x_2(k) \\ \vdots \\ x_N(k) \end{bmatrix} + \begin{bmatrix} \alpha_1 P_{13}^{\mathrm{T}} B_{e1}^{\mathrm{T}} B_{e2} \\ \vdots \\ \alpha_N P_{N3}^{\mathrm{T}} B_{e1}^{\mathrm{T}} B_{e2} \end{bmatrix}$$

$$\times\ \varrho(k+N_y) + \begin{bmatrix} b_1 P_{13}^{\mathrm{T}} + \alpha_1 P_{13}^{\mathrm{T}} B_{e1}^{\mathrm{T}} B_{e1} \\ \vdots \\ b_N P_{N3}^{\mathrm{T}} + \alpha_N P_{N3}^{\mathrm{T}} B_{e1}^{\mathrm{T}} B_{e1} \end{bmatrix} R(k+N_y) = 0.$$

Concretely, it results in

$$\sum_{j\in\mathcal{N}_i} w_{ij} P_{i3}^{\mathrm{T}} \hat{Y}_j(k+N_y|k) + \alpha_i P_{i3}^{\mathrm{T}} B_{e1}^{\mathrm{T}} B_{e1} R(k+N_y) + \alpha_i P_{i3}^{\mathrm{T}} B_{e1}^{\mathrm{T}}$$

$$\times B_{e2}\varrho(k+N_y) - \big((w_i+b_i)P_{i3}^{\mathrm{T}} + \alpha_i P_{i3}^{\mathrm{T}} B_{e1}^{\mathrm{T}} B_{e1}\big)\hat{Y}_i(k+N_y|k) = 0$$

that is

$$\begin{aligned}&\sum_{j\in\mathcal{N}_i} w_{ij} P_{i3}^{\mathrm{T}} \left(\hat{Y}_j(k+N_y|k) - \hat{Y}_i(k+N_y|k)\right) \\ &\quad + (b_i + 2\alpha_i) P_{i3}^{\mathrm{T}} \left(R(k+N_y) - \hat{Y}_i(k+N_y|k)\right) = 0\end{aligned}$$

such that

$$\begin{aligned}&\sum_{j\in\mathcal{N}_i} w_{ij} \left(\hat{Y}_j(k+N_y|k) - R(k+N_y)\right) \\ &\quad - (w_i + b_i + 2\alpha_i) \left(\hat{Y}_i(k+N_y) - R(k+N_y)\right) = 0\end{aligned}$$

which can be converted as

$$\Omega \begin{bmatrix} \hat{Y}_1(k+N_y|k) - R(k+N_y) \\ \vdots \\ \hat{Y}_N(k+N_y|k) - R(k+N_y) \end{bmatrix} = 0$$

with

$$\Omega = \begin{bmatrix} -(w_1 + b_1 + 2\alpha_1)I & \cdots & w_{1N} I \\ \vdots & \ddots & \vdots \\ w_{N1} I & \cdots & -(w_N + b_N + 2\alpha_N)I \end{bmatrix}.$$

When $\det(\Omega) \neq 0$, $\hat{Y}_i(k+N_y|k) = R(k+N_y), i \in \mathcal{N}$, which results in $\hat{Y}_i(k+N_y|k) = \hat{Y}_j(k+N_y|k), i \in \mathcal{N}, j \in \mathcal{N}_i$. With $k \to \infty$, $\lim_{k\to\infty} \|y_i(k) - y_j(k)\| = 0$, which holds Condition C2. Thus, system (4) realizes the stability and consensus.

Lemma 1 (See[41]): System (20) achieves the AS if and only if there is a Lyapunov function $\eta(\xi(k))$ such that the following statements hold.

1) $\eta(\xi(k))$ is positive definite.
2) $\Delta\eta(\xi(k+1))$ is negative definite.

Remark 2: In Remark 1, $\Delta\hat{V}(k+N_u|k)$ is further given as

$$\Delta\hat{V}(k+N_u|k)=\Delta\hat{V}_0(k+N_u|k)-F_0^{-1}\Xi^{\mathrm{T}}\left(\Xi F_0^{-1}\Xi^{\mathrm{T}}+\Lambda^{-1}\right)^{-1}\times\left(\Xi\Delta\hat{V}_0(k+N_u|k)-\Upsilon\right)$$

when $\Lambda\to\infty$, it is obtained as

$$\Delta\hat{V}(k+N_u|k)=\Delta\hat{V}_0(k+N_u|k)-F_0^{-1}\Xi^{\mathrm{T}}\left(\Xi F_0^{-1}\Xi^{\mathrm{T}}\right)^{-1}\times\left(\Xi\Delta\hat{V}_0(k+N_u|k)-\Upsilon\right)$$

such that

$$\begin{aligned}\Xi\Delta\hat{V}(k+N_u|k)&=\Xi\Delta\hat{V}_0(k+N_u|k)-\Xi F_0^{-1}\Xi^{\mathrm{T}}\left(\Xi F_0^{-1}\Xi^{\mathrm{T}}\right)^{-1}\\&\quad\times\left(\Xi\Delta\hat{V}_0(k+N_u|k)-\Upsilon\right)\\&=\Xi\Delta\hat{V}_0(k+N_u|k)-\Xi\Delta\hat{V}_0(k+N_u|k)+\Upsilon\\&=\Upsilon\end{aligned}$$

which means critical constraints can be satisfied when $\Lambda\to\infty$. Actually, input saturation and prescribed performance condition can be held when Λ is big enough in our view (see [40]), which is easy and simple to develop in practice. It also means the feasible region of $\Delta\hat{V}(k+N_u|k)$ is constructed via some solutions of $\Delta\hat{V}_0(k+N_u|k)$, its boundaries correspond to the critical values of constraints (12) and (13). When Λ is big enough, the critical conditions of constraints (12) and (13) are held, $\Delta\hat{V}_0(k+N_u|k)$ under this condition is located in the feasible region of $\Delta\hat{V}(k+N_u|k)$ (see [40] and [42]). However, a shortcoming in this work is that an explicitly analytical condition is difficult to present for the relationship between Λ and given constraints, it will be addressed along with our future and in-depth research. At present, only a personal experience for parameter selection is given as follows:

1) Choose w_i, b_i, α_i to ensure $\det(\Omega)\neq 0$.
2) α_i and β_i are big enough because $\Lambda=\text{Blockdiag}\{\Lambda_1,\ldots,\Lambda_N\}$, $\Lambda_i=\text{Blockdiag}\{\alpha_i I,\beta_i I\}$.

Remark 3: A guideline to solve the $\Delta v_i(k)$ in (17) is given as follows.

Step 1: Construct system (4) by designing a fully actuated control as $u_i(k)=B_i^{-1}v_i(k)$ for HOFAMAS (1).
Step 2: Convert system (4) into (6) and use a Diophantine (7) to establish an IHOFA prediction model (8) based on (6).
Step 3: Obtain multistep predictions via (8) and use them to transform constraints (2) and (3) into (12) and (13).
Step 4: Establish $J_i'(k)$ in (15) from $J_i(k)$ in (14) and choose the parameters to satisfy $\det(\Omega)\neq 0$, then optimize (15) to solve the $\Delta v_i(k)$ by (17).

V. Formation Control for ABS Simulators

A. Plant Model Description

An experimental platform of MASs is provided in Fig. 2, where the ABS simulator, given in Fig. 3, is a common simulated equipment to achieve the attitude joint orbit control of

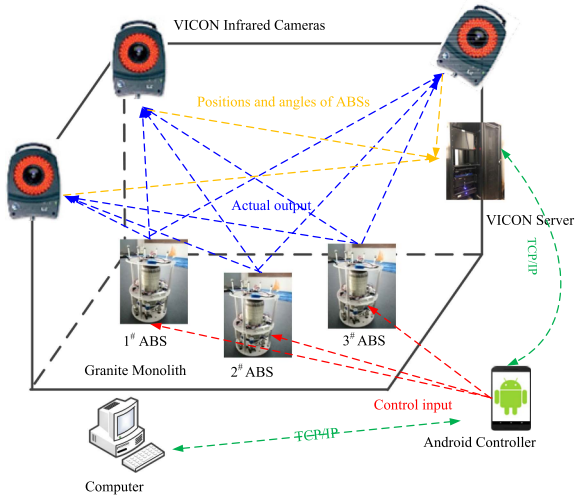

Fig. 2. Experimental platform.

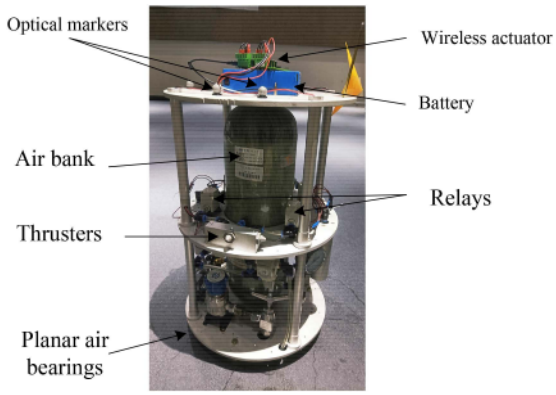

Fig. 3. Hardware of the ABS simulator.

spacecraft under microgravity site at ground (see [43], [44], and [45]), its achievements can be extended to practical spacecraft control, containing formation control, capture, flying-around, de-tumbling, rendezvous, docking, etc., which has great engineering values. In practice, the ABS simulator obtains three freedom degrees to be controlled, including x, y (positions in this plane), and ψ (angle rotating about the z-axis). In this platform, VICON Infrared Cameras collect the information of x, y, and ψ via optical markers of the ABS simulator and send them to VICON Server via network. Android Controller utilizes this information to calculate the control input for every ABS simulator. A supervisory control software on a computer is operated to achieve the monitoring and preservation of the real-time information. More details about this platform have been reported by our team in [33]. There are three ABS simulators in this experimental platform, that is, $\mathcal{N}=\{1,2,3\}$. Table I gives the related parameters of three ABS simulators,where $i=1,2,3$ denote $1^{\#}$, $2^{\#}$, and $3^{\#}$ ABS simulators. The practical environment on site is shown in Fig. 4. Let the coordinate origin locate at the center of Granite Monolith, a linearized dynamic model of the ith ABS simulator on x, y, and ψ axes are given as

$$m_i\ddot{x}_i=F_{xi},\ m_i\ddot{y}_i=F_{yi},\ J_i\ddot{\psi}=F_{Ti}\qquad(21)$$

TABLE I
RELATIVE PARAMETERS OF THREE ABS SIMULATORS

Equipment Number	Mass (m_i)	Moment of Inertia (J_i)
$1^{\#}$ ABS	19.4 kg	0.239 kg $\cdot$ m^2
$2^{\#}$ ABS	19.5 kg	0.241 kg $\cdot$ m^2
$3^{\#}$ ABS	19.2 kg	0.236 kg $\cdot$ m^2

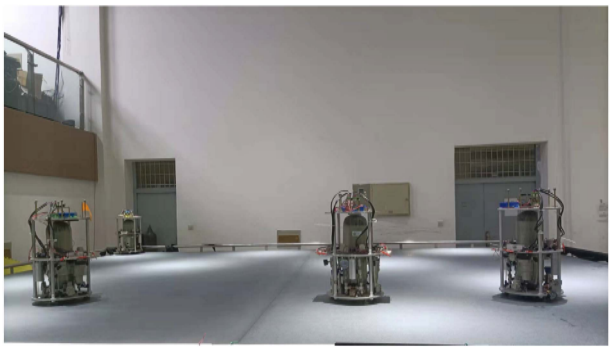

Fig. 4. Practical environment on site.

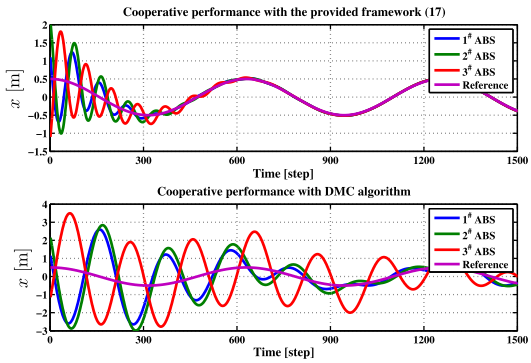

Fig. 5. Comparison of cooperative performance between the provided scheme (17) and the DMC algorithm.

where F_{xi}, F_{yi}, and F_{Ti} indicate the inputs on x, y, and ψ axes of the ith ABS simulator. Discretizing (21) yields a set of second-order fully actuated systems as

$$m_i x_i(k+2)-2m_i x_i(k+1)+m_i x_i(k) = T^2 F_{xi}(k) \quad (22a)$$

$$m_i y_i(k+2)-2m_i y_i(k+1)+m_i y_i(k) = T^2 F_{yi}(k) \quad (22b)$$

$$J_i \psi_i(k+2)-2J_i \psi_i(k+1)+J_i \psi_i(k) = T^2 F_{Ti}(k) \quad (22c)$$

where T denotes the sampling period. To offset the impacts of both packed losses and Ping delays of the network and to simplify the calculation, the sampling period is set to $T = 0.4$ s.

B. Simulated Comparison

System (22a) is taken as an illustration to compare with the dynamic matrix control (DMC) algorithm in [40]. Considering the power assignment of thrust distributors, constraint (2) for system (22a) is given as $-1 \le F_{xi}(k) \le 1$, and for constraint (3), a performance boundary function is provided as $\rho(k) = \coth(0.003k + 0.25) - 0.95$. For the presented work,

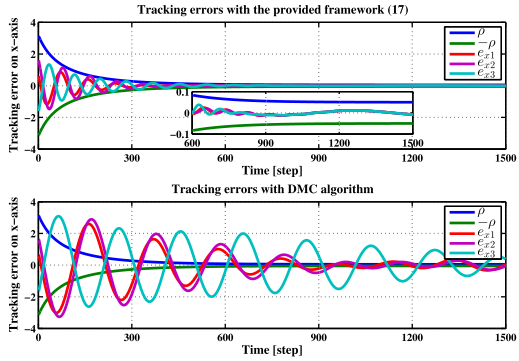

Fig. 6. Comparison of tracking errors on the x-axis between the provided scheme (17) and the DMC algorithm.

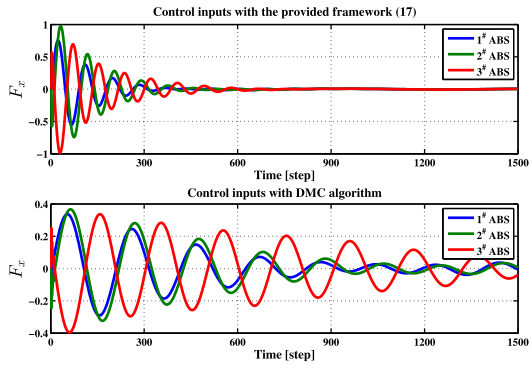

Fig. 7. Comparison of control inputs between the provided scheme (17) and the DMC algorithm.

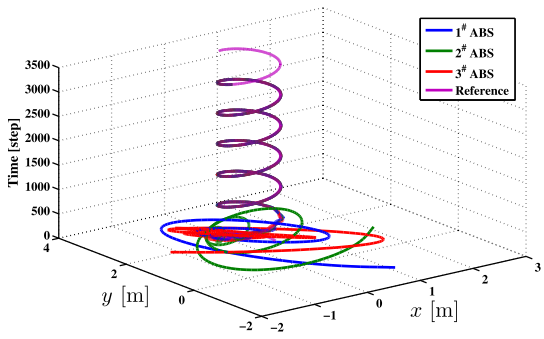

Fig. 8. Circular trajectory with the provided scheme (17).

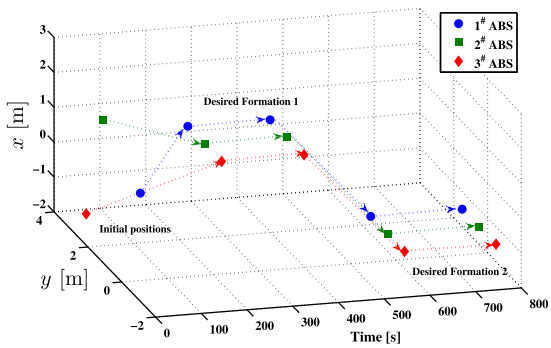

Fig. 9. Desired formation of three ABS simulators.

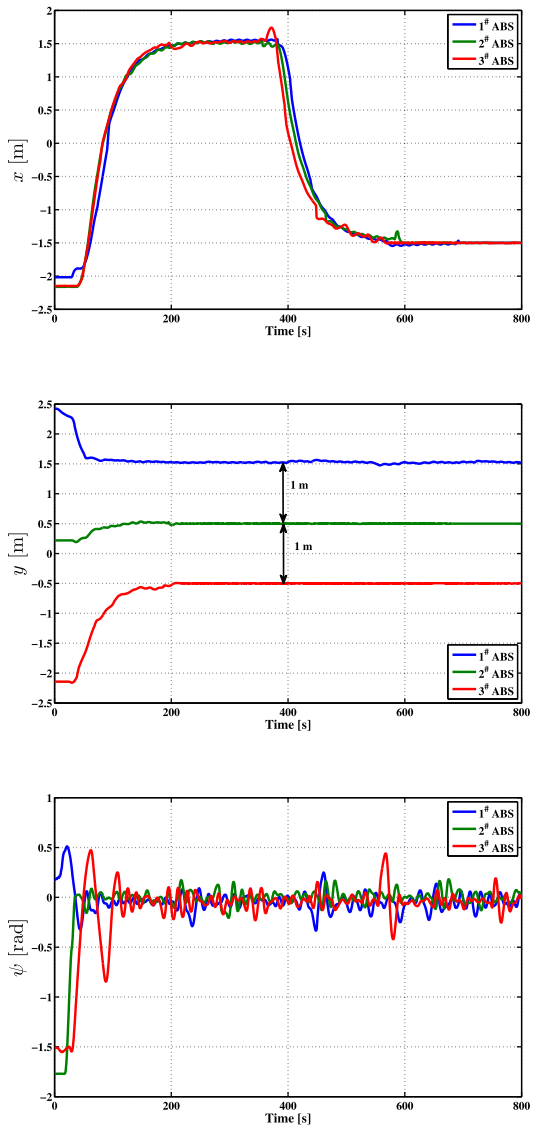

Fig. 10. Practical responses of the formation control experiment for three ABS simulators.

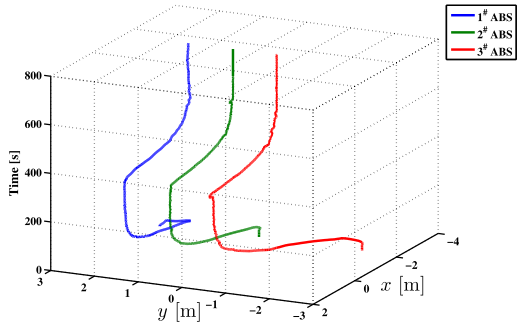

Fig. 11. Practical formation of three ABS simulators.

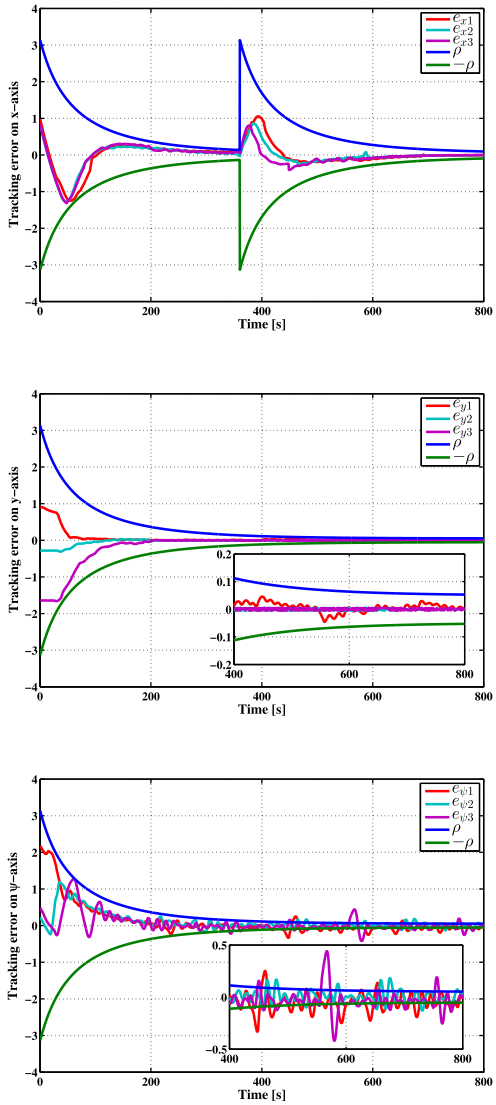

Fig. 12. Tracking errors on x, y, and ψ axes.

choose $N_y = 5$, $N_u = 3$ and $w_{ii} = 0$, $w_{ij} = 1$, $b_i = 1$, $c_i = 1$, $\alpha_i = 500$, $\beta_i = 100$, $\Gamma_i = I$, $i \in \mathcal{N}$, $j \in \mathcal{N}_i$. For DMC algorithm in [40], system (22a) is first transformed into a first-order expression as

$$X_i(k+1) = A_{xi}X_i(k) + B_{xi}F_{xi}(k)$$

with $X_i(k) = \begin{bmatrix} x_i(k) \\ x_i(k+1) \end{bmatrix}$, $A_{xi} = \begin{bmatrix} 0 & 1 \\ -1 & 2 \end{bmatrix}$, $B_{xi} = \begin{bmatrix} 0 \\ 0.0082 \end{bmatrix}$. Select the same parameters, prediction horizons, and constraints, the comparison results are shown in Figs. 5–7, where the reference input is given as $r_x(k) = 0.5\cos(\frac{1}{100}k)$.

Fig. 5 gives the comparison of the cooperative performance between the provided scheme (17) and the DMC algorithm, where the provided scheme (17) can realize both dynamical and steady cooperative performances, but DMC algorithm cannot guarantee the same performance. The tracking errors are provided in Fig. 6, which shows the provided scheme (17) can make the tracking errors be enclosed by the performance boundary function $\rho(k)$ with a rapid convergence rate; however, the DMC algorithm causes the tracking errors to go beyond $\rho(k)$. Fig. 7 provides the variation diagrams of control inputs that are clearly limited by the given saturation constraint while the DMC

algorithm can reduce the costs of control inputs compared to the provided scheme (17). Figs. 5–7 fully illustrate the effectiveness and benefits of the provided scheme, which offers a basis for practical application.

Based on the above conclusion, a flying-around simulation is considered whose reference trajectories are given as

$$r_{xi}(k) = 0.5\cos\left(\frac{1}{100}k + \frac{2(i-1)}{3}\pi\right)$$
$$r_{yi}(k) = 0.5\sin\left(\frac{1}{100}k + \frac{2(i-1)}{3}\pi\right) + 1.5$$

it means the desired trajectory is a circle with a radius of 0.5 and a center of $(0, 1.5)$. Select the same parameters, prediction horizons, and constraints, the simulated result is given in Fig. 8, which shows the provided scheme (17) can successfully perform the proposed flying-around mission; it means the dynamic cooperation subject to input saturation and prescribed performance can be implemented.

C. Experimental Results

To further test the theoretical result, a formation control experiment for three ABS simulators is performed, the desired formation is given in Fig. 9, where three ABS simulators first arrive at the desired formation 1 from initial positions and then reach the desired formation 2 from desired formation 1 with time going.

For systems (22a) and (22b), the parameters, prediction horizons, and constraints are chosen as the same as Section V-B, and for system (22c), choose $N_y = 5, N_u = 3$ and $w_{ii} = 0, w_{ij} = 1$, $b_i = 1$, $c_i = 1$, $\alpha_i = 5$, $\beta_i = 400$, $\Gamma_i = I$, $i \in \mathcal{N}$, $j \in \mathcal{N}_i$, and $-0.3 \le F_{Ti}(k) \le 0.3$, $\rho(k) = \coth(0.01k + 0.2) - 0.95$. The experimental results are given in Figs. 10–13 with the provided scheme (17).

Fig. 10 shows the practical responses of formation control experiment, where x and y axes responses simultaneously arrive at the specified positions with a tolerated error and can be cooperatively changed in dynamical process while a drawback is that there are jitters of the ψ-axis responses because of the airflow in the experimental site and reacting forces caused by thrusters. Fig. 11 clearly gives the practical formation for three ABS simulators; it illustrates that the provided predictive control scheme can successfully perform the formation mission. The tracking errors are shown in Fig. 12, where the errors on x and y axes are all enclosed by the performance boundary function $\rho(k)$, the reason there is a jump in the errors on the x-axis is that three ABS simulators receive an instruction to move from desired formation 1 to desired formation 2, the clock of $\rho(k)$ is reset to 0 at this moment. Meanwhile, the errors on the ψ-axis go beyond the $\rho(k)$, because of a common drawback of air-bearing equipment that the airflow in the experimental site and reacting forces cause the random and unpredictable jitters. Fig. 13 shows the variation diagrams of control inputs, which are limited within the given input saturation. The experimental results verify the effectiveness and superiority of the provided scheme in constrained cooperative control and its application in formation control, which offers a better foundation for extension in practical spacecraft control.

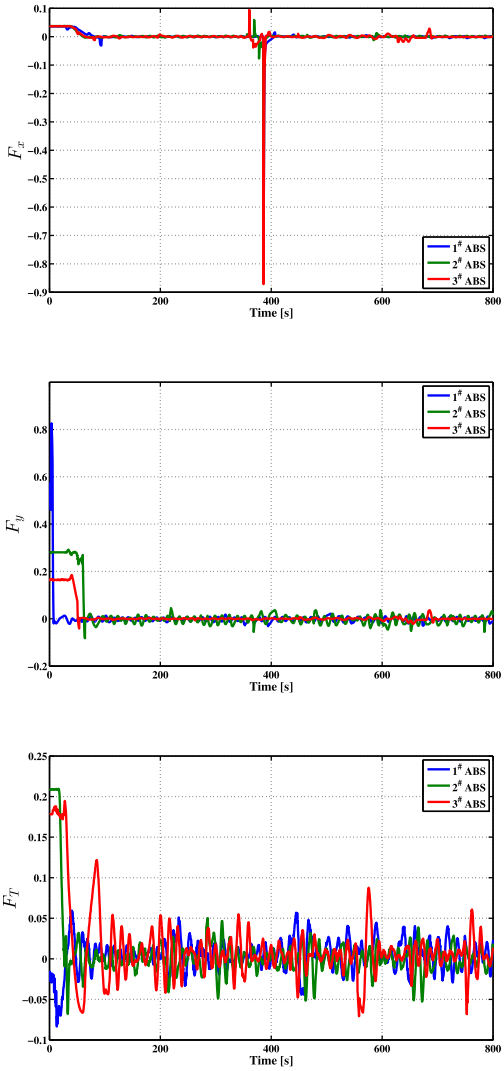

Fig. 13. Practical control inputs of a formation control experiment for three ABS simulators.

VI. Conclusion

In this study, a predictive control scheme has been provided for the constrained cooperative control for HOFAMASs subject to input saturation and prescribed performance. An IHOFA prediction model has been constructed by using Diophantine equation, which completes the multistep output predictions for the optimization of the cooperative performance and the implementation of given constraints about input saturation and prescribed performance. As a result, the stability and consensus have been effectively achieved. The future work will continue to construct an explicitly analytical condition on the relationship between design parameters and given constraints, and also pay attention to cooperative control for HOFAMASs with network constraints, including network-induced communication constraints, cyberattacks, game theories, etc.

REFERENCES

[1] S. Mahdavi, H. Panamtash, A. Dimitrovski, and Q. Zhou, "Predictive coordinated and cooperative voltage control for systems with high penetration of PV," *IEEE Trans. Ind. Appl.*, vol. 57, no. 3, pp. 2212–2222, May/Jun. 2021.

[2] W. Bai, Z. Lin, H. Dong, and B. Ning, "Distributed cooperative cruise control of multiple high-speed trains under a state-dependent information transmission topology," *IEEE Trans. Intell. Transp. Syst.*, vol. 20, no. 7, pp. 2750–2763, Jul. 2019.

[3] D. W. Zhang and G. P. Liu, "Coordinated control of quasilinear multiagent systems via output feedback predictive control," *ISA Trans.*, vol. 128, pp. 58–70, 2021, doi: 10.1016/j.isatra.2021.10.004.

[4] M. A. Kamel, X. Yu, and Y. Zhang, "Fault-tolerant cooperative control design of multiple wheeled mobile robots," *IEEE Trans. Control Syst. Technol.*, vol. 26, no. 2, pp. 756–764, Mar. 2018.

[5] W. Liu, S. Liu, J. Cao, Q. Wang, X. Lang, and T. Liu, "Learning communication for cooperation in dynamic agent-number environment," *IEEE/ASME Trans. Mechatronics*, vol. 26, no. 4, pp. 1846–1857, Aug. 2021.

[6] Q. M. Ta and C. C. Chea, "Multi-agent control for stochastic optical manipulation systems," *IEEE/ASME Trans. Mechatronics*, vol. 25, no. 4, pp. 1971–1979, Aug. 2020.

[7] V. P. Tran, F. Santoso, M. A. Garratt, and I. R. Petersen, "Distributed formation control using fuzzy self-tuning of strictly negative imaginary consensus controllers in aerial robotics," *IEEE/ASME Trans. Mechatronics*, vol. 26, no. 5, pp. 2306–2315, Oct. 2021.

[8] X. Li, W. Kong, and J. He, "A task-space form-finding algorithm for tensegrity robots," *IEEE Access*, vol. 8, pp. 100578–100585, 2020.

[9] R. Ji, B. Yang, J. Ma, and S. S. Ge, "Saturation-tolerant prescribed control for a class of MIMO nonlinear systems," *IEEE Trans. Cybern.*, vol. 52, no. 12, pp. 13012–13026, Dec. 2022, doi: 10.1109/TCYB.2021.3096939.

[10] R. Ji, D. Li, J. Ma, and S. S. Ge, "Saturation-tolerant prescribed control of MIMO systems with unknown control directions," *IEEE Trans. Fuzzy Syst.*, to be published, doi: 10.1109/TFUZZ.2022.3166244.

[11] K. Yong, M. Chen, Y. Shi, and Q. Wu, "Flexible performance-based robust control for a class of nonlinear systems with input saturation," *Automatica*, vol. 122, 2020, Art. no. 109268.

[12] D. Qi, J. Hu, X. Liang, J. Zhang, and Z. Zhang, "Research on consensus of multi-agent systems with and without input saturation constraints," *J. Syst. Eng. Electron.*, vol. 32, no. 4, pp. 947–955, 2021.

[13] B. Wang, W. Chen, J. Wang, B. Zhang, and P. Shi, "Semiglobal tracking cooperative control for multiagent systems with input saturation: A multiple saturation levels framework," *IEEE Trans. Autom. Control*, vol. 66, no. 3, pp. 1215–1222, Mar. 2021.

[14] L. Cao, H. Li, G. Dong, and R. Lu, "Event-triggered control for multiagent systems with sensor faults and input saturation," *IEEE Trans. Syst., Man, Cybern. Syst.*, vol. 51, no. 6, pp. 3855–3866, Jun. 2021.

[15] H. Chu, B. Yi, G. Zhang, and W. Zhang, "Performance improvement of consensus tracking for linear multiagent systems with input saturation: A gain scheduled approach," *IEEE Trans. Syst., Man, Cybern. Syst.*, vol. 50, no. 3, pp. 734–746, Mar. 2020.

[16] Y. Lv, J. Fu, G. Wen, T. Huang, and X. Yu, "On consensus of multiagent systems with input saturation: Fully distributed adaptive antiwindup protocol design approach," *IEEE Trans. Control Netw. Syst.*, vol. 7, no. 3, pp. 1127–1139, Sep. 2020.

[17] Z. Li and J. Zhao, "Adaptive consensus of non-strict feedback switched multi-agent systems with input saturation," *IEEE/CAA J. Autom. Sinica*, vol. 8, no. 11, pp. 1752–1761, Nov. 2021.

[18] Y. Li, Y. Liu, and S. Tong, "Observer-based neuro-adaptive optimized control of strict-feedback nonlinear systems with state constraints," *IEEE Trans. Neural Netw. Learn. Syst.*, vol. 33, no. 7, pp. 3131–3145, Jul. 2022, doi: 10.1109/TNNLS.2021.3051030.

[19] Y. Li, J. Zhang, W. Liu, and S. Tong, "Observer-based adaptive optimized control for stochastic nonlinear systems with input and state constraints," *IEEE Trans. Neural Netw. Learn. Syst.*, to be published, doi: 10.1109/TNNLS.2021.3087796.

[20] C. P. Bechlioulis and G. A. Rovithakis, "Robust adaptive control of feedback linearizable MIMO nonlinear systems with prescribed performance," *IEEE Trans. Autom. Control*, vol. 35, no. 9, pp. 2090–2099, Oct. 2008.

[21] Z. Lin, J. Yao, and W. Deng, "Input constraint control for hydraulic systems with asymptotic tracking," *ISA Trans.*, vol. 129, pp. 616–627, 2022, doi: 10.1016/j.isatra.2022.01.020.

[22] W. Deng and J. Yao, "Asymptotic tracking control of mechanical servosystems with mismatched uncertainties," *IEEE/ASME Trans. Mechatronics*, vol. 26, no. 4, pp. 2204–2214, Aug. 2021.

[23] Y. Yang, X. Si, D. Yue, and Y. C. Tian, "Time-varying formation tracking with prescribed performance for uncertain nonaffine nonlinear multiagent systems," *IEEE Trans. Automat. Sci. Eng.*, vol. 18, no. 4, pp. 1778–1789, Oct. 2021.

[24] F. Chen and D. V. Dimarogonas, "Leader–follower formation control with prescribed performance guarantees," *IEEE Trans. Control Netw. Syst.*, vol. 8, no. 1, pp. 450–461, Mar. 2021.

[25] C. E. Ren, J. Zhang, and Y. Guan, "Prescribed performance bipartite consensus control for stochastic nonlinear multiagent systems under event-triggered strategy," *IEEE Trans. Cybern.*, to be published, doi: 10.1109/TCYB.2021.3119066.

[26] H. Liang, Y. Zhang, T. Huang, and H. Ma, "Prescribed performance cooperative control for multiagent systems with input quantization," *IEEE Trans. Cybern.*, vol. 50, no. 5, pp. 1810–1819, May 2020.

[27] Y. Liu and G. H. Yang, "Prescribed performance-based consensus of nonlinear multiagent systems with unknown control directions and switching networks," *IEEE Trans. Syst., Man, Cybern. Syst.*, vol. 50, no. 2, pp. 609–616, Feb. 2020.

[28] G. Dong, H. Ren, D. Yao, H. Li, and R. Lu, "Prescribed performance consensus fuzzy control of multiagent systems with nonaffine nonlinear faults," *IEEE Trans. Fuzzy Syst.*, vol. 29, no. 12, pp. 3936–3946, Dec. 2021.

[29] S. L. Dai, S. He, Y. Ma, and C. Yuan, "Distributed cooperative learning control of uncertain multiagent systems with prescribed performance and preserved connectivity," *IEEE Trans. Neural Netw. Learn. Syst.*, vol. 32, no. 7, pp. 3217–3229, Jul. 2021.

[30] Y. Cao and Y. Song, "Performance guaranteed consensus tracking control of nonlinear multiagent systems: A finite-time function-based approach," *IEEE Trans. Neural Netw. Learn. Syst.*, vol. 32, no. 4, pp. 1536–1546, Apr. 2021.

[31] G. R. Duan, "High-order fully actuated systems approaches: Part I. Models and basic procedure," *Int. J. Syst. Sci.*, vol. 52, no. 2, pp. 422–435, 2021.

[32] G. P. Liu, "Coordination of networked nonlinear multi-agents using a high order fully-actuated predictive control strategy," *IEEE/CAA J. Autom. Sinica*, vol. 9, no. 4, pp. 615–623, Apr. 2022.

[33] D. W. Zhang, G. P. Liu, and L. Cao, "Coordinated control of high-order fully actuated multiagent systems and its application: A predictive control strategy," *IEEE/ASME Trans. Mechatronics*, to be published, doi: 10.1109/TMECH.2022.3156587.

[34] D. W. Zhang, G. P. Liu, and L. Cao, "Proportional integral predictive control of high-order fully actuated networked multiagent systems with communication delays," *IEEE Trans. Syst., Man, Cybern. Syst.*, to be published, doi: 10.1109/TSMC.2022.3188504.

[35] G. P. Liu, "Coordinated control of networked multiagent systems via distributed cloud computing using multistep state predictors," *IEEE Trans. Cybern.*, vol. 52, no. 2, pp. 810–820, Feb. 2022.

[36] Z. H. Pang, W. C. Luo, G. P. Liu, and Q. L. Han, "Observer-based incremental predictive control of networked multi-agent systems with random delays and packet dropouts," *IEEE Trans. Circuits Syst. II: Exp. Briefs*, vol. 68, no. 1, pp. 426–430, Jan. 2021.

[37] Z. H. Pang, C. B. Zheng, C. Li, G. P. Liu, and Q. L. Han, "Cloud-based time-varying formation predictive control of multi-agent systems with random communication constraints and quantized signals," *IEEE Trans. Circuits Syst. II: Exp. Briefs*, vol. 69, no. 3, pp. 1282–1286, Mar. 2022.

[38] G. R. Duan, "High-order fully actuated systems approaches: Part X. Basics of discrete-time systems," *Int. J. Syst. Sci.*, vol. 53, no. 4, pp. 810–832, 2022.

[39] D. W. Zhang and G. P. Liu, "Constrained control of networked high-order fully actuated systems via predictive control," in *Proc. 41st Chin. Control Conf.*, 2022, pp. 4366–4371.

[40] Y. G. Xi, *Predictive Control (in Chinese)*, 2nd ed. Beijing, China: Nat. Defense Ind. Press, 2013.

[41] K. Ogata, *Discrete-Time Control System*, 2nd ed. Upper Saddle River, NJ, USA: Prentice-Hall, 1995.

[42] D. M. Prett and R. D. Gillete, "Optimization and constrained multivariable control of a catalytic cracking unit," in *Proc. Joint Amer. Control Conf.*, 1980, Art. no. WP5-C.

[43] C. Papakonstantinou, G. Moraitis, V. Lappas, and V. Kostopoulos, "Design of a low-cost air bearing testbed for nano CMG maneuvers," *Aerospace*, vol. 9, no. 2, 2022, Art. no. 95.

[44] T. Rybus, M. Wojtunik, and F. L. Basmadji, "Optimal collision-free path planning of a free-floating space robot using spline-based trajectories," *Acta Astronautica*, vol. 190, pp. 395–408, 2022.

[45] Y. Eun, S. Y. Park, T. Lee, and G. N. Kim, "Experimental validation of positive adaptive-control approach for spacecraft proximity maneuvers," *J. Aerosp. Eng.*, vol. 34, no. 6, 2021, Art. no. 04021096.

Da-Wei Zhang (Student Member, IEEE) received the B.S. degree in electrical engineering and automation from the China University of Mining and Technology, Xuzhou, China, in 2017, and the M.S. degree in control science and engineering from Northeast Electric Power University, Jilin, China, in 2020. He is currently working toward the Ph.D. degree in control science and engineering with the Department of Control Science and Engineering, Harbin Institute of Technology, Harbin, China.

His research interests include high-order fully actuated systems, predictive control, cooperative control of networked multiagent systems, and their applications.

Guo-Ping Liu (Fellow, IEEE) received the B.Eng. and M.Eng. degrees in automation from Central South University, Changsha, China, in 1982 and 1985, respectively, and the Ph.D. degree in control engineering from the University of Manchester, Manchester, U.K., in 1992.

He is currently a Professor with the Southern University of Science and Technology, Shenzhen, China. He has authored or coauthored more than 400 journal papers and 10 books on control systems. His current research interests include networked multiagent control systems, nonlinear system identification and control, advanced control of industrial systems, and multiobjective optimization and control.

Prof. Liu is a member of Academia Europaea and an IET Fellow.

Lei Cao received the B.S. degree in mechanical engineering from the Nanjing University of Aeronautics and Astronautics, Nanjing, China, in 2014, and the M.S. degree in mechanical engineering from Nanchang University, Nanchang, China, in 2018. He is currently working toward the Ph.D. degree in control science and engineering with the Department of Control Science and Engineering, Harbin Institute of Technology, Harbin, China.

His current research interests include networked control systems and Android-based remote laboratories.